THE ASTROPHYSICAL JOURNAL, 407:470–488, 1993 April 20

ALL-SKY CATALOGS OF SUPERCLUSTERS OF ABELL-ACO CLUSTERS

ELENA ZUCCA
Dipartimento di Astronomia, Università di Bologna, via Zamboni 33, 40126 Bologna, Italy, and Istituto di Radioastronomia/CNR, via Irnerio 46, 40126 Bologna, Italy
GIOVANNI ZAMORANI
Osservatorio Astronomico, via Zamboni 33, 40126 Bologna, Italy, and Istituto di Radioastronomia/CNR, via Irnerio 46, 40126 Bologna, Italy
ROBERTO SCARAMELLA
Osservatorio Astronomico di Roma, 00040 Monteporzio Catone, Italy
AND
GIAMPAOLO VETTOLANI
Istituto di Radioastronomia/CNR, via Irnerio 46, 40126 Bologna, Italy
Received 1992 July 24; accepted 1992 October 19

ABSTRACT

We present the results of a statistical analysis of structures in the Abell and ACO catalogs of clusters of galaxies. For both catalogs we have improved upon distance estimates for clusters without measured radial velocity and we discuss in detail the calibration of the magnitude-redshift relation.

Through a percolation analysis we have obtained catalogs of superclusters at various density excesses: we analyze their reality and global properties, focusing in particular on the problem of the possible existence of large peculiar motions of clusters in superclusters. We find (in agreement with recent similar studies) that these systems do not appear to be preferentially elongated along the radial direction and we derive an upper limit of ~ 1000 km s^{-1} for velocity dispersion of clusters in superclusters.

Subject headings: catalogs — galaxies: clustering — galaxies: distances and redshifts

1. INTRODUCTION

With the publication in 1958 of the Abell catalog of galaxy clusters (Abell 1958, hereafter the Abell catalog) it has become evident that, like galaxies, rich clusters themselves are not randomly distributed throughout the space, but tend to group together into larger systems (see Bahcall 1988 for a review). Several authors have derived catalogs of superclusters and have studied their properties (e.g., Bahcall & Soneira 1984; Batuski & Burns 1985a; West 1989; Postman, Huchra, & Geller 1992). With the recent publication of the southern extension of the Abell catalog (Abell, Corwin, & Olowin 1989, hereafter the ACO catalog) a sample of clusters covering (almost) the whole sky has become available and a comparison of the selection effects affecting the two catalogs has become possible (see for example Scaramella et al. 1991; Cappi & Maurogordato 1992).

The aim of the present work is to obtain an all-sky catalog of superclusters, inside a distance of $\sim 300\ h^{-1}$ Mpc, using the whole Abell-ACO catalog, through a percolation algorithm which individuates density enhancements of clusters over the mean density. After having obtained supercluster catalogs at various density excesses, we analyze their reality and global properties, focusing in particular on the problem of the possible existence of large peculiar motions of clusters in superclusters (see Bahcall, Soneira, & Burgett 1986; Soltan 1988; Huchra et al. 1990; Postman et al. 1992; Rood 1992).

In § 2 we describe the samples and we derive, through a magnitude-redshift relation, distance estimates for clusters without measured radial velocities; in § 3 we present our supercluster catalogs and we describe the method of selection. In § 4 we analyze the supercluster properties and we compare them with random catalogs; moreover, we deal with the problem of peculiar motions in superclusters, through the study of both the separations of pairs of clusters belonging to superclusters and the use of the inertia tensor of each supercluster. Finally, in § 5 we summarize our results.

2. THE SAMPLE AND DISTANCE ESTIMATES

2.1. *The Abell-ACO Catalog*

The Abell catalog of rich clusters of galaxies contains a total of 2712 clusters north of declination $\delta \geq -27°$. Its extension (ACO catalog; Abell et al. 1989) contains 1638 clusters south of declination $\delta \leq -17°$ and completes the sky coverage. These two catalogs, although similar in many respects, show however some important differences. A detailed comparison of the properties of the two catalogs can be found in Scaramella et al. (1991, hereafter SZVC). Following SZVC we have eliminated from the ACO catalog all the clusters with less than 30 members; all these clusters, but one, lie in the overlap region, thus suggesting that they have been included in the ACO catalog only because they had been previously found by Abell and included in the northern catalog. Moreover, we excluded from our analysis three clusters (A3208, A3833, and A3897) which are the same objects as A3207, A3832, and A2462, respectively (see ACO paper). After these exclusions the ACO catalog lists 1607 clusters.

The percentage of clusters with measured redshift is significantly smaller for the clusters of the ACO catalog (245 measured redshifts out of 1607, corresponding to $\sim 15.2\%$) than for the clusters of the Abell catalog (829 out of 2712, corresponding to $\sim 30.6\%$). In compiling our catalog of measured redshifts we have heavily relied on the compilation of Struble & Rood (1991) and on the data of the complete sample ($m_{10} \leq 16.5$) of Postman et al. (1992). In particular, we have paid attention to correct our data according to Table 2 of Struble & Rood (1991), which gives a list of redshifts previously assigned

incorrectly to Abell clusters. These references have been supplemented by additional "sparse" data found in the literature or through private communications.

2.2. *Distance Estimates*

In order to study the spatial distribution of the Abell-ACO clusters, we need distance estimates for clusters without measured radial velocities. Following what has been done in the past by various authors and by SZVC, we used the clusters with measured redshifts to calibrate a magnitude-redshift relation.

In particular, following SZVC, we have fitted, separately for the Abell and ACO catalogs, the following relation:

$$f(z) \equiv \log [D_L(z)] + 0.2K(z) = A + Bg(m) + C \log (N_g) , \quad (1)$$

where $D_L(z)$ is the luminosity distance and $K(z)$ is the K-correction. In the first place we have used for the Abell clusters $K(z) = 1.122z$ (Postman et al. 1985) and for the ACO ones $K(z) = 4.14z - 0.44z^2$ (Ellis 1983; Shanks et al. 1984; but see discussion of this point later on). Both relations are appropriate for elliptical and S0 galaxies, which are the most likely morphological types for the brightest members in a rich cluster; the difference between the two adopted K-corrections is due to the different plate material used for the search of clusters in the two catalogs. The quantity $g(m)$ is a function of the magnitudes corrected for extinction. For the Abell magnitudes we have adopted the correction that was originally applied by Abell; for the ACO catalog we have used the equation derived by Fisher & Tully (1981). While for the Abell catalog we have been forced to use $g(m) = m_{10}$, m_{10} being the only magnitude listed in this catalog, for the ACO catalog (which lists m_1, m_3, and m_{10}) we have adopted $g(m) = 0.5(m_3 + m_{10})$ (see SZVC). Finally, the last term on the right side of equation (1), where N_g is the number of galaxies of the clusters as reported in the Abell and ACO catalogs, is a correction for the so-called Scott effect (see Postman et al. 1985), i.e., the fact that richer clusters have systematically brighter M_{10}.

The luminosity distance D_L has been computed through the Mattig (1958) expression

$$D_L = \frac{c}{H_0} \frac{q_0 z + (q_0 - 1)(\sqrt{1 + 2q_0 z} - 1)}{q_0^2} , \quad (2)$$

where we have assumed $H_0 = 100$ km s^{-1} Mpc^{-1} and $q_0 = 0.5$. Different values for q_0 have small effect (at most a few percent) at the distances which are of interest here.

Note that, strictly speaking, the coefficient in front of the K-correction term should be the quantity B and not the theoretically assumed value 0.2, so that an iterative procedure would in principle be more appropriate. However, as long as the derived value of B differs little from 0.2 (see below), the difference with respect to the above formula will be a quite negligible quantity.

We then defined the sample variance estimate as

$$\sigma^2_{\text{sample}} = \sum_{i=1}^{N_{\text{obj}}} (f_{i,\text{meas}} - f_i)^2/(N_{\text{obj}} - \nu) ,$$

where N_{obj} is the number of calibrating objects and ν is the number of parameters in the fitted functional relationship (here $\nu = 3$). In fitting the relation we have excluded "discrepant" clusters, defined as the clusters whose measured redshifts differ from the estimated ones more than the number of σ above which only 0.25 objects are expected in a Gaussian distribution. This number of σ is 3.61 and 3.29 for the Abell and ACO catalogs respectively, and the excluded clusters are A261, A484, A536, A2661 (in Abell) and A2539, A2911, A3354, A3593, A3740, A3742 (in ACO).

After these exclusions we have obtained the following parameters from the fit

$$A = -4.9917 \pm 0.0830 \quad B = 0.2245 \pm 0.0055$$
$$C = 0.1734 \pm 0.0256$$
$$\sigma_{\text{sample}} = 0.1327 \quad N_{\text{obj}} = 825 \quad (3)$$

for the Abell catalog, and

$$A = -4.5004 \pm 0.0930 \quad B = 0.2001 \pm 0.0052$$
$$C = 0.1453 \pm 0.0355$$
$$\sigma_{\text{sample}} = 0.1044 \quad N_{\text{obj}} = 329 \quad (4)$$

for the ACO catalog.

The errors represent the projections onto the parameter axes of the 1 σ confidence ellipsoid in the (A, B, C) space. Note that the parameter B differs only by $\sim 12\%$ (in Abell) and $\sim 0.05\%$ (in ACO) from the theoretical value 0.2, thus justifying the previous assumption on the coefficient of the K-correction term. These best-fit parameters are consistent with those derived by SZVC, although the number of measured redshifts now available is substantially higher than those used in SZVC's analysis.

For what concerns the K-correction term, it is interesting to note that the inclusion of this term in equation (1), although requested by the theory, increases by $\sim 10\%$ the sample variance estimate. This behavior is not a consequence of the redshift incompleteness: even if we fit relation (1) on the Abell sample with $m_{10} \leq 16.5$, which is complete in redshift, the case without the K-correction term still has a smaller σ_{sample}.

Equation (1) is correct only if the absolute magnitudes of the objects which are used in the calibration are constant with redshift, i.e., can be considered standard candles. In order to check this assumption, we have plotted the absolute magnitudes [M_{10} for the Abell sample and $0.5(M_3 + M_{10})$ for the ACO sample], corrected only for K-dimming, against the measured redshifts. Although the absolute magnitude, in principle, should not depend on z, we find that, especially for the Abell sample, there is a significant correlation between M_{10} and redshift, with M_{10} being systematically brighter at higher redshifts. This trend is probably due to the combined result of the presence of the Scott effect, of a Malmquist bias, of errors on the measurements of faint m_{10}, and possibly of other unknown selection effects. The existence of this correlation prompted us to introduce an additional term in equation (1) which empirically corrects for the observed correlation between absolute magnitudes and redshift. We then assumed a correction to the absolute magnitudes which is a linear function of the redshift, and fitted a new relation:

$$\log [D_L(z)] + 0.2(\alpha + K)z = A' + B'g(m) + C' \log (N_g) , \quad (5)$$

where α is the slope of the absolute magnitude-redshift relation and K is the linear coefficient of the K-correction term. Henceforth we neglect the small contribution of the quadratic term in the K-correction for the ACO catalog.

The correction to the absolute magnitudes has been obtained through an iterative procedure. First we have dealt with the Scott effect, by fitting relation (1) *without* the K-correction term and obtaining the parameter for the Scott

effect correction. Then we have computed the absolute magnitudes (corrected only for the Scott effect) and plotted them versus the redshift (Figs. 1*a* and 1*b*). The fact that the observed trend of the absolute magnitude with redshift is significantly stronger for the Abell sample suggests that magnitude errors (whose presence in this catalog was already noticed by Corwin 1974) may be the main reason for the observed relation. The milder effect seen in the ACO sample is therefore due to the much more accurate magnitudes, together with the use of an average of two magnitudes (m_3 and m_{10}). Notice also that the fact that the slope of the absolute magnitude-redshift relation for the ACO clusters is positive is not due to an opposite behavior of the correction for the two catalogs: in fact the slope in Figure 1 corresponds to $(K + \alpha)$ (being the plotted magnitudes computed without K-correction), and even if α is negative for both Abell and ACO, in the ACO catalog we have $K > |\alpha|$, and therefore the slope is positive. This effect can be seen by comparing the solid lines, which are a linear fit to the data, with the dashed lines which show the expected relation between absolute magnitude and redshift induced by the assumed K-correction only (i.e., $\alpha = 0$).

After the correction for the Scott effect, we have then substituted the obtained $(K + \alpha)$ in relation (5), and we have iterated this procedure, slightly varying $(K + \alpha)$, until the slope of the absolute magnitude-redshift relation is ~ 0. The latter condition is satisfied for $(K + \alpha) = -5.15$ and $+0.5$ for the Abell and ACO catalogs, respectively. By comparing these values with the originally adopted parameters for the K-correction (see § 2.2), it results that $\alpha_{\rm Abell} \sim -6.3$ and $\alpha_{\rm ACO} \sim -3.6$. The new absolute magnitude-redshift relations at the end of this procedure are shown in Figures 2*a* and 2*b*. Correspondingly, the new values of the parameters obtained by fitting relation (5) are

$$A' = -4.0189 \pm 0.0562 \quad B' = 0.1644 \pm 0.0037$$
$$C' = 0.1046 \pm 0.0174$$
$$\sigma_{\rm sample} = 0.0899 \quad N_{\rm obj} = 825 \qquad (6)$$

for the Abell catalog, and

$$A' = -4.1720 \pm 0.0838 \quad B' = 0.1779 \pm 0.0047$$
$$C' = 0.1253 \pm 0.0320$$
$$\sigma_{\rm sample} = 0.0941 \quad N_{\rm obj} = 239 \qquad (7)$$

for the ACO catalog. In both cases the "discrepant" clusters are the same as in the fit of relation (1). Figures 3*a* and 3*b* show $z_{\rm fit}$ versus $z_{\rm true}$ for Abell and ACO catalogs, respectively; crosses represent the "discrepant" clusters eliminated from the fit. In comparing the dispersions $\sigma_{\rm sample}$ obtained by fitting equation (5) with those resulting from the fit to equation (1) it is clear that $\sigma_{\rm sample}$ has decreased for both samples, implying a better defined fitting relation. This is particularly true for the Abell sample, whose $\sigma_{\rm sample}$ has decreased by more than 30% and is of the same order as that of the ACO sample. For both samples these new fitting relations appear to hold up to $z \sim 0.2$.

Finally, we have analyzed the distributions of the redshift residuals. Figures 4*a* and 4*b* show $\log (z_{\rm fit}/z_{\rm true})$ versus $z_{\rm true}$ for Abell and ACO catalogs, respectively. In both panels it is visible, although much more pronounced in Abell, a trend of the residuals with redshift: the residuals are on average positive at low redshift and negative at high redshift. Postman et al. (1985) attributed this distribution of the residuals to contamination from foreground galaxies either in the redshift measurements (positive residuals at low redshift) or in m_{10} measurements (negative residuals at high redshift). Alternatively, we suggest that, although some foreground contamination may well be present in these data, this fact alone is not the correct explanation for the distribution of the residuals. In fact, we suggest that the observed trend of the residuals with $z_{\rm true}$ is naturally expected any time that residuals (e.g., $y_{\rm fit} - y_{\rm true}$) are plotted versus $y_{\rm true}$, where $y_{\rm fit}$ is the result of a least-square fit of a variable y versus x. In fact, in fitting y versus x the distribution of the residuals is expected to be flat when plotted versus $y_{\rm fit}$ and *not* versus $y_{\rm true}$ (see Isobe et al. 1990 for a general discussion about linear regression in

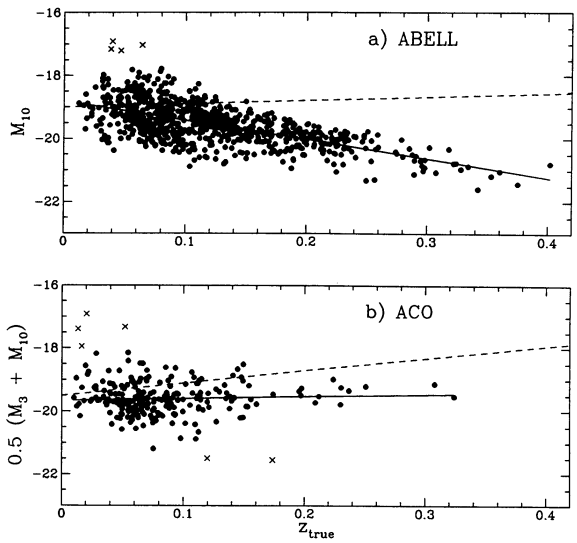

FIG. 1.—Dependence on the redshift of the absolute magnitude M_{10} for the Abell catalog (*a*) and $0.5\,(M_3 + M_{10})$ for the ACO catalog (*b*). The magnitudes are corrected *only* for Scott effect. Solid lines are linear fits to the data, dashed lines show the expected relation between absolute magnitude and redshift induced by the assumed K-correction only (at $z = 0$ the values of $M_{10} = -19$ and $0.5(M_3 + M_{10}) = -19.5$ have been assumed). Crosses (×) represent "discrepant" clusters eliminated from the fits.

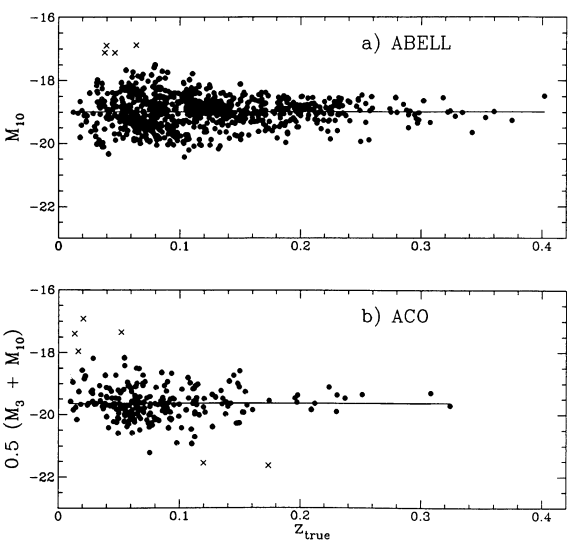

FIG. 2.—Same as Fig. 1 after having applied the $(K + \alpha)$ correction (see text) to the magnitudes. Solid lines are linear fits to the data. Crosses (×) represent "discrepant" clusters eliminated from the fits.

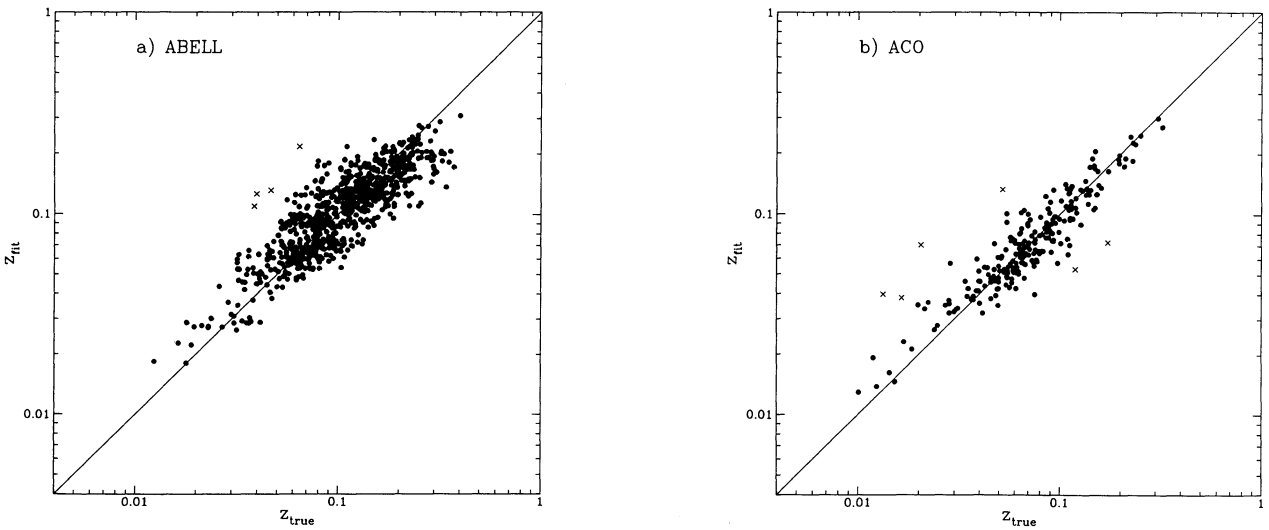

FIG. 3.—Plot of z_{fit} vs. z_{true} for the Abell (*a*) and ACO (*b*) catalog. Crosses (×) represent "discrepant" clusters eliminated from the fit of the magnitude-redshift relations. Solid lines represent $z_{fit} = z_{true}$.

astronomy). Figures 4*c* and 4*d*, where the residuals log (z_{fit}/z_{true}) are plotted versus z_{fit}, clearly demonstrate that this is verified for both the Abell and the ACO samples.

3. SUPERCLUSTERING

3.1. *Separation between Clusters*

Having calibrated the magnitude-redshift relation for Abell and ACO catalogs, we have then used the derived parameters (eq. [6] and [7]) to estimate the distance from us of the clusters without measured redshift:

$$D(\mathrm{Mpc}) = R_0 r = \frac{c}{H_0} \frac{q_0 z + (q_0 - 1)(\sqrt{1 + 2q_0 z} - 1)}{q_0^2(1 + z)}, \quad (8)$$

where r is the comoving coordinate distance (computed through the Mattig 1958 expression) and R_0 is the scale factor at the present time.

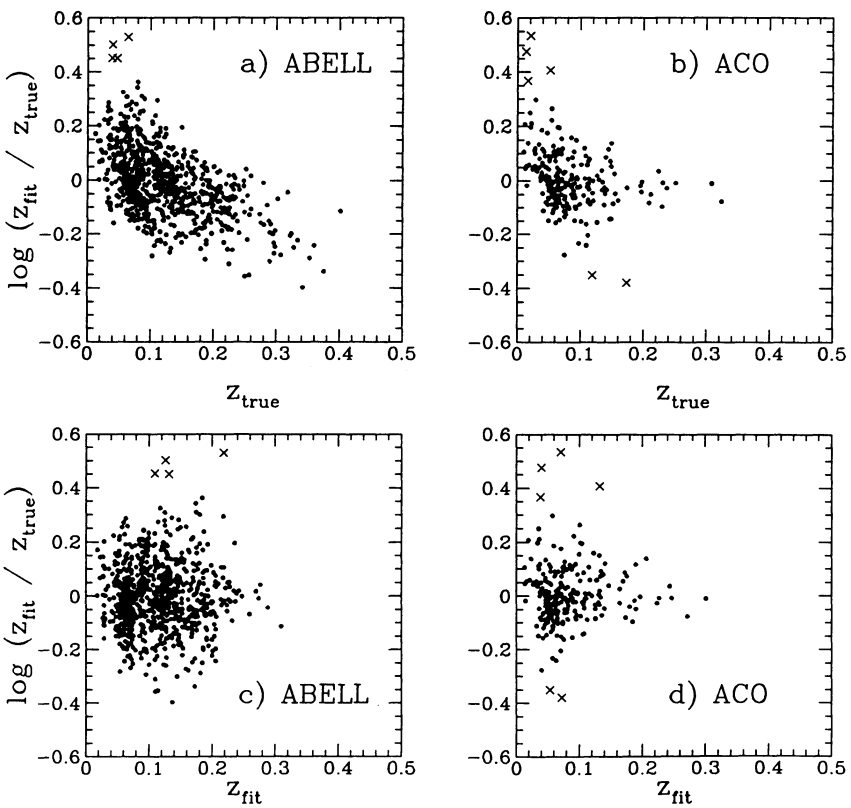

FIG. 4.—Distribution of the redshift residuals log (z_{fit}/z_{true}) vs. z_{true} for the Abell (*a*) and ACO (*b*) catalogs. In both panels a trend of the residuals with the redshift is visible, but this trend disappears when the residuals log (z_{fit}/z_{true}) are plotted vs. z_{fit} (*c* and *d*).

The next step is to compute the comoving distance s which separates two clusters at redshifts z_1 and z_2 and with angular separation θ. The general method to calculate the distance between objects separated by arbitrary large redshifts or angular distances has been derived by Osmer (1981). However, since approximate expressions (valid only in the low redshift and/or small angular distance limits) are often used in similar applications, we briefly describe it here. The main ingredient of the method is the translation of the coordinate system (in the Robertson-Walker metric) from the Earth to one of the objects, using the transformation formula (Weinberg 1972, p. 413, eq. [14.2.7])

$$\boldsymbol{X}' = \boldsymbol{X} + \boldsymbol{a}\left[\sqrt{1 - k\boldsymbol{X}^2} - (1 - \sqrt{1 - k\boldsymbol{a}^2})\left(\frac{\boldsymbol{X}\cdot\boldsymbol{a}}{\boldsymbol{a}^2}\right)\right], \quad (9)$$

where $\boldsymbol{X}'$ and $\boldsymbol{X}$ are the spatial distance vectors measured from the new and the old origin respectively, $\boldsymbol{a}$ is the translation vector as measured from the new origin and k is the curvature term in the Robertson-Walker metric. The problem of finding the distance between two clusters simply reduces to translating the coordinate system on one of the two objects; the distance is then given by the magnitude of the transformed vector $\boldsymbol{X}'$, being $\boldsymbol{X}$ the coordinate vector of the second object in the old system. Note that, being the distances expressed in comoving coordinates, the derived separation is independent from the choice of the starting cluster, i.e., the distance computed from the first to the second cluster is equal to that computed from the second to the first.

As shown by Osmer (1981), the simplest way to use equation (9) is to locate each pair of objects in the observer's (x, y, z) coordinate frame at $(0, 0, r_1)$ and $(r_2 \sin\theta, 0, r_2 \cos\theta)$, where r_1 and r_2 are the comoving distances of the first and the second cluster, respectively. With this choice of coordinate $\boldsymbol{a} = (0, 0, -r_1)$ and the comoving separation between the two objects is

$$\boldsymbol{s} = (r_2 \sin\theta, 0, r_2 \cos\theta) + (0, 0, -r_1) \times \left[\sqrt{1 - kr_2^2} + \frac{r_2}{r_1}\cos\theta - \frac{r_2}{r_1}\cos\theta\sqrt{1 - kr_1^2}\right]. \quad (10)$$

Only for $q_0 = 0.5$, equation (10) reduces to the standard Euclidean cosine rule:

$$|\boldsymbol{s}| = \sqrt{r_1^2 + r_2^2 - r_1 r_2 \cos\theta}\,. \quad (11)$$

The comoving separation can then be transformed to a metric separation in Mpc, at a given time t, by multiplying it for the scale factor $R(t)$. In the following, metric separations will be always referred to the present time.

3.2. *Method of Selection*

The criterion we adopted to construct our samples of superclusters is based on the individuation, through a percolation algorithm, of cluster density enhancements over the mean density, at various levels of overdensity f. If in a sphere of radius r_p around a cluster there are $N(r \le r_p)$ clusters, the local density is

$$n(r \le r_p) = \frac{N(r \le r_p)}{4/3\pi r_p^3} \quad (12)$$

In the ideal case of a constant cluster density n_0, one can define a local density enhancement as $f = (n/n_0)$, where n_0 is the mean cluster density in the whole sample; it results that in the sphere of radius r_p the overdensity f is given by

$$f = \frac{N(r \le r_p)}{4/3\pi r_p^3 n_0} \quad (13)$$

Therefore, a given radius r_p will individuate different density enhancements around different clusters, depending on the local density. The presence of a single cluster in the sphere of radius r_p individuates the minimum density enhancement

$$f_{\min} = \left(\frac{4}{3}\pi r_p^3 n_0\right)^{-1} \quad (14)$$

Therefore, for each overdensity f a percolation radius

$$r_p = \left(\frac{4}{3}\pi f n_0\right)^{-1/3} \quad (15)$$

would individuate superclusters with a density enhancement greater than or equal to f.

Since the observed cluster density is not constant through the whole sample, but depends on the position in the sky (see SZVC for a detailed discussion), we have "corrected" equation (15) through a selection function

$$n(b^{\rm II}, \zeta) = n_0\, 10^{-a(\mathrm{cosec}\,|b^{\rm II}| - 1)} 10^{-b(\sec|\zeta| - 1)}, \quad (16)$$

where $\zeta = \delta - \delta_{\rm tel}$ is the zenithal angle, i.e., the difference between the object declination and the earth latitude of the telescope site. SZVC derived the parameters n_0, a, and b for both Abell and ACO catalogs (see the parameters for the volume selection function in their Table 3). Because of the substantially increased number of measured redshifts now available for the ACO clusters, we have recomputed the parameters for the ACO sample; the differences between the new and the old values are well within the 1 σ uncertainties. Our final adopted parameters for the volume limited samples are

$$n_0 = 14.6(\pm 1.2) \times 10^{-6}\ h^3\ \mathrm{Mpc}^{-3};$$
$$a = 0.20 \pm 0.07; \quad b = 0.18 \pm 0.09 \text{ for Abell};$$
$$n_0 = 25.2(\pm 1.5) \times 10^{-6}\ h^3\ \mathrm{Mpc}^{-3};$$
$$a = 0.32 \pm 0.04; \quad b = 0.60 \pm 0.18 \text{ for ACO}.$$

Therefore for each cluster we use the following variable percolation radius:

$$r_p = \left[\frac{4}{3}\pi f n(b^{\rm II}, \zeta)\right]^{-1/3}. \quad (17)$$

The fact that, for any given f, r_p, being a function of the local density, is different for different clusters, implies that the construction of the percolation chains is not a unique process; in fact, given two clusters i and j, separated by a distance r_{ij} and with $r_p(i) < r_{ij} < r_p(j)$, it would happen that the two clusters are connected in chain when starting from cluster j, while they are not connected when starting from cluster i. In order to avoid this ambiguity, we have considered as connected two clusters only when

$$r_{ij} \le \frac{r_p(i) + r_p(j)}{2}. \quad (18)$$

Weighting the percolation radius with the inverse of the selection function may be dangerous in regions where the selection function becomes excessively small, thus producing very large

percolation radii. To avoid this problem, we have eliminated from our analysis those clusters with $|b^{II}| < 15°$: this implies the exclusion of A63, A426, A553, A581, A619, A2319 in the Abell catalog and A3394, A3409, A3410, A3411, A3412, A3463, A3589, A3602, A3627 in the ACO one. At $|b^{II}| = 15°$ the average value of the selection function is of the order of 0.25 and 0.10 for the Abell and ACO samples, respectively.

The individuation of superclusters through the presence of "local" density excesses allows us to use the union of Abell and ACO catalogs as a single sample: in fact, given f, the variable percolation radius takes into account the different density of the two catalogs. The only possible ambiguity is for the clusters located in the overlap region; we have considered these clusters as being members of the ACO catalog, which in this region appears to be more complete than the Abell catalog (see SZVC).

3.3. *The Superclusters*

In order to quantitatively study how the selection of superclusters is affected by the assumed value of f, we performed the analysis for various f, ranging from $f \geq 1.5$ to $f \geq 400$. The catalogs for $f \geq 2$, 10, 20, 40, 200 are shown in Table 1: column (1) gives the sequential number of the supercluster, column (2) the identification number of the supercluster in the $f \geq 2$ catalog and column (3) its members; the numbers in italic denote clusters with estimated redshift. Columns (4) and (5), (6) and (7), (8) and (9), and (10) and (11), are the same as columns (2) and (3) for $f \geq 10$, 20, 40, 200, respectively. The last two columns give the correspondence of our superclusters with those of Postman, Huchra, & Geller (1992, hereafter code PHG) and Cappi & Maurogordato (1992, hereafter code CM). Table 1 gives also, for each value of f, two values of r_p (in h^{-1} Mpc) which represent the percolation radius corresponding to $n(b^{II}, \zeta) = n_0$ for the Abell and ACO catalogs, respectively: these values represent the lower limit to r_p, being n_0 the maximum value that the selection function can assume. Notice that a direct comparison between our supercluster catalogs and those of Bahcall & Soneira (1984), for similar f values, is not possible: in fact, they derived for each cluster a radius r_m which individuates a given f, but they considered two clusters as connected if their distance is less than $2r_m$, instead of $1r_m$ as in our standard percolation procedure. Therefore their values of f are significantly higher than ours and, on average, must be scaled down by a factor ~ 8 in order to be comparable to our density excesses.

The total number of superclusters in our $f \geq 2$ catalog is 69, significantly higher than the number of superclusters listed by PHG (23 superclusters) and CM (24 superclusters). Most of the difference is due to the larger areas (and volumes) used in our analysis. In the overlap area the agreement between our catalog and the PHG and CM ones is fairly good. Comparing the three catalogs at $f \geq 2$ (although the CM catalog is at $f \geq 1.9$) we see that there is only one PHG supercluster (PHG3) and two CM superclusters (N2 ≡ PHG3 and N6) which do not appear in our list: we find both these superclusters at a slightly lower density excess.

Vice versa, there are some superclusters which appear in our catalog and are not present in PHG and/or CM lists, even if their coordinates and distance are within the limits of PHG and/or CM catalogs. This is mainly due to the fact that in the percolation procedure we use also clusters with estimated redshift; secondly, in regions near the boundaries (both in coordinates and in distance) of the PHG and/or CM samples the exclusion of clusters just outside the limits can lead to a loss of superclusters; finally, especially for low $|b^{II}|$, our variable percolation radius can produce superclusters which PHG and/or CM miss.

Although a significant number of the listed superclusters has most of the members with measured redshift, there still is a non-negligible fraction of possible supercluster members whose redshift has been estimated through the relations given in § 2. Since the statistical significance of these systems is obviously related to the percentage of members with measured redshift, in the following we will apply our tests both on all the superclusters and only on those with more than 70% of the members with measured redshift.

Our supercluster catalogs have been obtained using clusters of all richness classes, with the only constraint of $|b^{II}| > 15°$. We have also limited our catalogs to superclusters with mean distance (computed as the average of single cluster distances) smaller than 300 h^{-1} Mpc, because for greater distances the Abell-ACO catalog is incomplete and the percentage of measured redshifts decreases significantly. Because of this limit, it is possible to lose superclusters in going from high to low f: this is the case for supercluster 46 in Table 1, which is in the $f \geq 10$ catalog (with a distance of 286.82 h^{-1} Mpc) but at $f \geq 2$ collects new more distant members, so that the mean distance goes over the limit. For $f \geq 100$ we have listed superclusters with two or more members; for lower density excesses we have listed only superclusters with three or more members. Because of this choice, it is possible that a supercluster with two members, which appears in the catalogs at high f, is not present in the lists at lower density excesses.

Considering in particular the $f \geq 2$ catalog, we summarize in Table 2 some properties of each supercluster. Columns (1) through (7) give the identification number, the mean α- and δ-coordinates and the mean distance of the supercluster computed as the average of single cluster coordinates, the number of clusters and the number of galaxies, which is simply the sum of the number of galaxies (as listed in the Abell-ACO catalog) of each cluster, and the percentage of clusters in each supercluster with measured redshift. The last three columns give the maximum extension (in h^{-1} Mpc) in α, δ, and distance, respectively. These extensions have been computed as the difference between the maximum and the minimum value of the three coordinates of all the members, without taking into account the supercluster shape, and therefore they represent only an indicative value of the supercluster dimensions.

3.4. *Specific Superclusters*

There are several studies in the literature dealing with supercluster identifications (and their reality), mostly confined to the northern Abell sample. The first studies to use a well defined density enhancement criterion are those by Thuan (1980) and Bahcall & Soneira (1984), however limited, because of the small number of available redshifts, to small volumes or rich clusters. Batuski & Burns (1985a) provided a large list of candidate superclusters from the Abell catalog, but in their study a fairly large (30 h^{-1} Mpc) percolation radius has been used. This can lead to the artificial linking of independent systems and to excessively huge superclusters. It must be stressed that the physical significance of every supercluster here as well as in all the other supercluster catalogs must be confirmed through the detection, in redshift space, of bridges or clouds of galaxies connecting the different clusters. This up to now is limited to a few well studied superclusters, as the Hercules Supercluster or the Perseus-Pisces (which, however, does not appear in the present list due to its low Galactic latitude).

TABLE 1

SUPERCLUSTER CATALOGS AT $f \geq 2, f \geq 10, f \geq 20, f \geq 40, f \geq 200$

# SC	#	$f \geq 2$ $r_p = 20.14; 16.79$	#	$f \geq 10$ $r_p = 11.78; 9.82$	#	$f \geq 20$ $r_p = 9.35; 7.79$	#	$f \geq 40$ $r_p = 7.42; 6.19$	#	$f \geq 200$ $r_p = 4.34; 3.62$	identifications PHG	CM
1	1/2	*7,2687,2702*	...	...	...	...	...	...	...	...		
2	...	...	...	...	...	...	...	...	1/200	**71,77**		
3	2/2	**14,74,80,86,114,133,2716, 2734,2800,2824,4053**	1/10 2/10	**74,80,86,2800** **114,133,2824**	... 1/20	... **114,133,2824**	...	...	...	...	13	S1
4	3/2	**76,119,147,160,168,193,195**	3/10	**119,147,168**	...	...	...	...	...	...	16	S4
5	4/2	**85,117,151**	...	...	...	...	...	...	...	...	14	S2
6	5/2	**102,116,134**	...	...	...	...	...	...	...	...	15	S3
7	6/2	**150,154,158,171, 225,257,292,311**	...	...	...	...	...	...	...	...	17	S5
8	7/2	*208,229,237*,**266**,*267,268, 271*,**277,281**,*295,303*	4/10	*267,268,271,295,303*	...	...	...	...	...	...		
9	8/2	**419,428,3094,3095**	...	...	...	...	...	...	...	...	18	S6
10	9/2	**548,3341,3367,3374**	...	...	...	...	...	...	2/200	**548,3367**	19	
11	10/2	*550,3358*,**3368**	...	...	...	...	...	...	...	...		
12	11/2	*575,625,737,809,848*	...	...	...	...	...	...	...	...		
13	...	...	...	...	...	...	...	...	3/200	*605*,**610**		
14	12/2	**690,692,699**	...	...	...	...	...	...	...	...		
15	13/2	**754,780,838,912,957**	...	...	...	...	...	...	...	...		
16	14/2	**930,970,978,979,993,1069**	5/10	**930,978,979,993**	2/20	**978,979,993**	1/40	**978,979,993**	4/200	**978,993**	1	
17	15/2	*971,1021,1067*	...	...	...	...	...	...	...	...		
18	16/2	**999,1016,1139,1142**	...	...	...	...	...	...	5/200	**999,1016**	2	N1
19	17/2	**1060,3526,3537, 3565,3574,3581**	24/10	**3526,3537,3565,3574**	...	...	...	...	...	...		

TABLE 1—*Continued*

# SC	#	$f \geq 2$ r_p = 20.14; 16.79	#	$f \geq 10$ r_p = 11.78; 9.82	#	$f \geq 20$ r_p = 9.35; 7.79	#	$f \geq 40$ r_p = 7.42; 6.19	#	$f \geq 200$ r_p = 4.34; 3.62	identifications PHG	CM
20	18/2	**1177,1185,1228,1257,1267**	6/10	**1177,1185,1267**	...	...	...	...	...	...	4	N3
21	19/2	**1216,1308,1334**	...	...	...	...	...	...	...	...	5	N4
22	20/2	**1291,1318,1377,1383, 1436,1452,1507**	7/10	**1291,1318,1377,1383**	...	...	...	...	...	...	6	N5
23	21/2	**1307,1337,1385,1390**	8/10	**1337,1385,1390**	...	...	...	...	...	...		
24	22/2	*1376,1389*,**1399**,*1404*	9/10	*1376,1389*,**1399**,*1404*	3/20	*1389*,**1399**,*1404*	2/40	*1389*,**1399**,*1404*	7/200	**1399**,*1404*		
25	23/2	**1474,1526,1541, 1552,1569,1589**	...	...	...	...	...	...	...	...		
26	24/2	**1709,1736,3528,3530, 3532,3542,***3548*,**3553 3554,3555,3556,3558, 3559,3560,***3561*,**3562, ***3563*,**3564,3566,3570 3571,3572,3575,3577,3578**	25/10	**3528,3530,3532**	11/20	**3528,3530,3532**	7/40	**3528,3530,3532**	21/200	**3528,3530,3532**	Shapley concentration	
			26/10	**3542,3553,3555, 3556,3558,3559, 3560,3562,3564, 3566**	12/20	**3542,3553,3555, 3556,3558,3559, 3560,3562,3564, 3566**	8/40	**3555,3556,3558, 3559,3560,3562, 3564,3566**	22/200	**3556,3558**		
									23/200	**3560,3562**		
									24/200	**3564,3566**		
			27/10	**3570,3571,3572,3575**	13/20	**3571,3572,3575**	9/40	**3571,3572,3575**	25/200	**3571,3572,3575**		
27	25/2	**1771,***1794*,*1802*	10/10	**1771,***1794*,*1802*	...	...	...	...	...	...		
28	26/2	**1773,1780,1809**	...	...	...	...	...	...	8/200	**1773,1780**		
29	27/2	**1775,1800,1873**	...	...	...	...	...	...	...	...	7	N7
30	28/2	**1781,1795,1825, 1827,1828,1831**	...	...	...	...	...	...	...	...	8	N8
31	...	...	...	...	...	...	...	...	9/200	*2017*,**2021**		
32	...	...	...	...	...	...	...	...	10/200	**2052,2063**		
33	29/2	**2019,2056,2061,2065,2067, 2079,2089,2092,2122,2124**	12/10	**2056,2061,2067**	...	...	...	...	...	...	10	N10
			...	...	...	...	...	...	11/200	**2122,2124**		
34	30/2	**2028,2029,2033**	11/10	**2028,2029,2033**	...	...	...	...	...	...		
35	31/2	**2107,2147,2148,2151, 2152,2162,2197,2199**	13/10	**2147,2151,2152**	4/20	**2147,2151,2152**	3/40	**2147,2151,2152**	12/200	**2151,2152**	9	N9
			...	...	...	...	...	...	13/200	**2197,2199**		
36	32/2	**2168,2169,2184**	...	...	...	...	...	...	...	...	11	N11

1993ApJ...407..470Z

TABLE 1—*Continued*

# SC	#	$f \geq 2$ $r_p = 20.14; 16.79$	#	$f \geq 10$ $r_p = 11.78; 9.82$	#	$f \geq 20$ $r_p = 9.35; 7.79$	#	$f \geq 40$ $r_p = 7.42; 6.19$	#	$f \geq 200$ $r_p = 4.34; 3.62$	identifications PHG	CM
37	33/2	**2248,2256,2271, 2295,2296,2309**	14/10	**2256,2271,2296**	5/20	**2256,2271,2296**	...	...	14/200	**2256,2271**	12	
38	34/2	**2301,2304,2311, 2312,2315**	15/10	**2301,2304,2311, 2312,2315**	...	...	...	...	15/200	**2301,2304**		
					6/20	**2311,2312,2315**	...	...	...	...		
39	35/2	**2361,2362,2372,2382,2401**	...	...	...	...	...	...	16/200	**2361,2362**		
40	36/2	**2366,2399,2415**	...	...	...	...	...	...	...	...	20	S7
41	37/2	**2377,2400,2402,2410,2420**	16/10	**2377,2402,2410**	...	...	...	...	17/200	**2402,2410**		
42	38/2	**2459,2462,2492**	...	...	...	...	...	...	...	...	21	S8
43	39/2	**2511,2525,2559,2597,2638**	...	...	...	...	...	...	...	...		
44	40/2	**2538,2556,2566,*3985***	...	...	...	...	...	...	...	...		
45	41/2	**2572,2589,2593,2657**	17/10	**2572,2589,2593**	7/20	**2572,2589,2593**	4/40	**2572,2589,2593**	...	...	22	S9
46	...	...	18/10	*2596,2599,2600*	...	...	...	...	...	...		
47	42/2	**2619,*2637,2640***	...	...	...	...	...	...	...	...		
48	43/2	**2622,2625,2626**	...	...	...	...	...	...	...	...	23	
49	44/2	**2731,2806,2870,2877,2911**	...	...	...	...	...	...	...	...		S10
50	45/2	*2732,4051*,**4067**	...	...	...	...	...	...	...	...		
51	46/2	**2801,*2804,2814,2829***	19/10	**2801,*2814,2829***	...	...	...	...	...	...		
52	47/2	*2836*,**2841,2854,2889**	20/10	*2836*,**2841,2854**	8/20	*2836*,**2841,2854**	5/40	*2836*,**2841,2854**	...	...		
53	...	...	...	...	...	...	...	...	18/200	**3004,3009**		
54	48/2	*3074*,**3078,3093**,*3100, 3104*,**3106,3108,3109,3110, 3112,3120,3122,3123,3125 3128**,*3133*,**3158,3164**	21/10	**3093**,*3100,3104*,**3108**	9/20	*3100,3104*,**3108**	...	...	...	...		S11 Horologium Reticulum
55	49/2	*3141,3154,3161,3195*	...	...	...	...	...	...	...	...		
56	50/2	**3144,3193,3202**	...	...	...	...	...	...	...	...		S12

TABLE 1—*Continued*

# SC	#	$f \geq 2$ r_p = 20.14; 16.79	#	$f \geq 10$ r_p = 11.78; 9.82	#	$f \geq 20$ r_p = 9.35; 7.79	#	$f \geq 40$ r_p = 7.42; 6.19	#	$f \geq 200$ r_p = 4.34; 3.62	identifications PHG	CM
57	51/2	*3146,3159,3166*	22/10	*3146,3159,3166*	10/20	*3146,3159,3166*	6/40	*3146,3159,3166*	19/200	*3159,3166*		
58	52/2	*3152,3153,3173,3183*	...	...	...	...	...	...	...	...		
59	53/2	*3191,3241,3242*	...	...	...	...	...	...	...	...		
60	54/2	*3256,3265,3268,3273, 3275,3285,3289,***3295**,*3307*	23/10	*3265,3273,3275*	...	...	...	...	...	...		
61	55/2	**3380,3391,3395**,*3407,3408*	...	...	...	...	...	...	20/200	*3407,3408*		
62	56/2	*3428,3432,3443*	...	...	...	...	...	...	...	...		
63	57/2	*3466,3476,3482*	...	...	...	...	...	...	...	...		
64	58/2	*3489,3490,3492,3501*	...	...	...	...	...	...	...	...		
65	59/2	*3494,3504,3508*	...	...	...	...	...	...	...	...		
66	60/2	*3524,***3531**,*3549*	...	...	...	...	...	...	...	...		
67	61/2	*3624,3626,***3629**	28/10	*3624,3626,***3629**	...	...	...	...	...	...		
68	62/2	**3651,3653,3667**	...	...	...	...	...	...	...	...		
69	63/2	**3656,3698,3742**	...	...	...	...	...	...	...	...		
70	64/2	*3677,3681,***3682**, *3690,***3691**,*3693,* **3694,3695,3696,3705**	29/10	*3677,***3691**,*3693,* **3695,3696,3705**	15/20	*3693,***3695**, **3696,3705**	10/40	*3693,***3695,3696**	...	...		
			30/10	*3681,***3682**,*3690,***3694**	14/20	*3681,3690,***3694**	...	...	...	...		
71	65/2	*3751,3755,***3756**,*3774*	...	...	...	...	...	...	...	...		
72	66/2	*3767,3772,3775*	...	...	...	...	...	...	26/200	*3772,3775*		
73	67/2	**3771,3785,3796,3806, 3822,3825,3826**,*3867*,**3886**	31/10	**3806,3822,3825,3826**	16/20	**3806,3822,3826**	...	...	...	...		S13
74	68/2	*3916,3932,3986,***3992**,*4066*	...	...	...	...	...	...	...	...		
75	69/2	*4021,4029,***4068**	...	...	...	...	...	...	...	...		
76	...	...	...	...	...	...	...	...	27/200	**4038,4049**		

TABLE 2

GLOBAL PROPERTIES OF THE SUPERCLUSTERS AT $f \geq 2$

SC	$\langle\alpha\rangle_{SC}$	$\langle\delta\rangle_{SC}$	$\langle$distance$\rangle_{SC}$ (Mpc)	N_{cl}	N_{gal}	z_{meas}	$(\Delta\alpha)_{max}$ (Mpc)	$(\Delta\delta)_{max}$ (Mpc)	$(\Delta$ distance$)_{max}$ (Mpc)
1/2.....	$0^h02^m58^s$	31°42′40″	296.4	3	139	33%	12.8	5.3	35.9
2/2.....	0 29 14	−24 29 16	181.6	11	528	100	49.3	23.9	40.9
3/2.....	1 06 35	7 04 09	128.7	7	356	100	26.3	46.4	18.5
4/2.....	0 53 00	−11 52 00	156.4	3	171	100	18.2	16.6	5.8
5/2.....	0 53 18	−0 26 40	190.1	3	130	100	11.9	12.9	18.2
6/2.....	1 30 50	16 42 07	189.1	8	388	100	47.5	21.7	30.0
7/2.....	1 48 57	−2 19 33	260.9	11	501	27	39.5	41.7	31.9
8/2.....	3 09 56	−24 23 30	190.7	4	200	100	5.7	26.8	8.7
9/2.....	5 42 40	−25 45 30	123.0	4	239	100	15.1	22.3	30.2
10/2.....	5 45 00	−21 25 40	259.8	3	194	33	15.2	8.6	20.9
11/2.....	8 48 48	78 54 36	299.3	5	265	0	35.3	38.9	27.8
12/2.....	8 38 34	27 58 00	238.7	3	140	100	5.0	8.7	29.0
13/2.....	9 37 25	−5 05 36	143.5	5	262	100	40.8	32.0	26.9
14/2.....	10 18 42	−7 07 50	162.3	6	279	100	23.2	16.3	26.2
15/2.....	10 26 45	39 52 40	267.8	3	163	0	18.7	15.4	4.9
16/2.....	10 39 43	9 13 45	102.2	4	141	100	16.6	20.3	22.2
17/2.....	12 57 14	−31 50 00	43.4	6	249	100	35.6	10.8	33.1
18/2.....	11 16 29	29 39 00	97.5	5	213	100	6.8	23.3	13.1
19/2.....	11 27 16	−3 58 39	150.2	3	133	100	13.8	1.3	20.9
20/2.....	11 49 19	55 53 34	167.6	7	384	100	18.1	24.1	35.0
21/2.....	11 39 52	12 23 59	234.5	4	204	100	16.8	17.9	2.1
22/2.....	11 47 13	−1 24 45	259.2	4	211	25	6.9	16.4	8.7
23/2.....	12 25 00	14 21 10	227.6	6	343	100	32.5	38.8	47.5
24/2.....	13 25 32	−32 32 36	137.9	25	1856	88	32.1	55.1	100.3
25/2.....	13 45 16	−26 13 00	298.5	3	215	33	10.7	2.3	5.0
26/2.....	13 44 09	3 40 40	222.2	3	215	100	10.8	11.2	3.7
27/2.....	13 52 09	27 46 20	213.5	3	173	100	24.7	6.6	14.0
28/2.....	13 52 13	24 26 30	181.0	6	399	100	10.6	36.3	15.0
29/2.....	15 25 14	30 40 12	206.0	10	626	100	32.8	32.1	44.2
30/2.....	15 08 11	6 44 20	223.1	3	172	100	1.8	6.9	13.1
31/2.....	16 06 05	26 02 37	102.7	8	489	100	19.9	45.5	30.5
32/2.....	16 14 45	51 17 00	168.0	3	142	100	3.6	14.8	17.6
33/2.....	17 41 17	76 24 50	165.2	6	276	100	17.7	27.6	42.7
34/2.....	18 40 03	69 24 24	253.9	5	268	100	17.9	8.9	16.3
35/2.....	21 44 21	−17 06 00	172.8	5	271	100	13.8	17.7	20.9
36/2.....	21 52 38	−6 59 20	165.1	3	139	100	16.2	6.3	12.4
37/2.....	21 56 17	−10 53 24	233.9	5	324	100	24.5	9.9	19.9
38/2.....	22 39 24	−17 40 40	203.6	3	123	100	11.8	12.8	10.3
39/2.....	23 13 40	−11 24 48	228.2	5	301	100	40.7	24.2	20.5
40/2.....	23 10 44	−21 34 30	235.2	4	238	75	6.9	14.2	13.2
41/2.....	23 25 25	14 33 45	118.6	4	165	100	13.2	19.9	4.5
42/2.....	23 35 21	20 45 20	277.7	3	161	33	7.4	11.2	14.1
43/2.....	23 33 24	22 45 40	172.5	3	133	100	1.1	20.8	13.2
44/2.....	0 52 29	−49 03 24	73.6	5	211	100	16.1	24.7	30.9
45/2.....	23 58 20	−62 53 40	286.0	3	147	33	9.5	18.8	13.0
46/2.....	0 40 46	−29 03 30	263.0	4	232	25	12.8	2.5	13.1
47/2.....	0 58 51	−49 10 00	185.7	4	205	75	11.2	9.5	7.4
48/2.....	3 18 43	−50 01 40	181.1	18	1063	78	24.6	53.4	54.8
49/2.....	3 43 48	−32 53 15	204.2	4	169	0	16.7	27.1	22.5
50/2.....	3 50 34	−53 49 20	111.9	3	160	100	6.7	5.3	23.5
51/2.....	3 41 6	−33 03 20	277.9	3	212	0	8.5	2.4	1.6
52/2.....	3 44 19	−33 18 00	235.6	4	190	0	12.1	9.3	21.5
53/2.....	4 09 50	−63 52 00	282.9	3	136	0	11.1	9.6	10.4
54/2.....	4 38 44	−34 48 07	288.4	9	466	11	37.0	39.2	47.1
55/2.....	6 37 39	−51 07 36	142.8	5	232	60	24.1	13.4	38.3
56/2.....	10 02 56	−33 15 20	210.5	3	211	0	21.7	2.6	25.7
57/2.....	11 13 48	−32 02 20	286.7	3	105	0	15.4	11.3	7.6
58/2.....	11 48 58	−31 40 30	224.4	4	198	0	18.8	22.8	25.1
59/2.....	12 04 36	−32 32 20	294.9	3	110	0	20.2	5.7	20.4
60/2.....	12 54 28	−31 55 40	220.0	3	135	33	27.9	18.3	9.9
61/2.....	16 08 16	−83 07 40	231.6	3	103	33	5.2	5.2	23.1
62/2.....	19 55 09	−54 46 40	153.2	3	202	100	7.8	12.9	31.4
63/2.....	20 31 09	−37 09 20	54.0	3	141	100	12.5	20.9	9.9
64/2.....	20 30 05	−35 19 42	250.7	10	740	60	13.6	20.5	37.8
65/2.....	21 15 53	−43 41 30	237.2	4	151	25	12.7	10.2	35.8
66/2.....	21 26 16	−43 07 40	289.0	3	189	0	4.1	3.3	13.0
67/2.....	21 51 38	−55 47 00	214.3	9	567	89	32.9	36.0	23.2
68/2.....	23 12 29	−73 08 48	274.2	5	171	20	24.8	15.2	32.9
69/2.....	23 44 34	−38 53 40	279.8	3	140	33	20.6	6.7	9.6

In the following we will briefly describe some of the richest superclusters in Table 2. The superclusters are referred to with their numbers in the $f \geq 2$ catalog (column [2] of Table 1).

SC 2/2 through SC 7/2 are part of the large Pisces-Cetus supercluster identified by Tully (1986) at a percolation radius $\gtrsim 40\ h^{-1}$ Mpc (see also Tully et al. 1992). This supercluster, at the density contrast considered here, is split into several parts. SC 2/2 and SC 7/2 are quite rich (11 clusters each); however, for most of the SC 7/2 clusters the radial velocities are only estimated. SC 3/2 represents the distant edge of a roughly spherical void with a diameter of $\simeq 40\ h^{-1}$ Mpc (Batuski & Burns 1988).

SC 20/2 represents the core of the Ursa Major supercluster as identified by Tully (1987).

SC 24/2 is the so-called Shapley Concentration,[1] first pointed out by Scaramella et al. (1989) and described in detail by Raychaudhury (1989) and Vettolani et al. (1990). This cluster complex is the richest supercluster known. It is dominated, at high density, by some dense cores: SC 25/200 with three members at $\sim 120\ h^{-1}$ Mpc, SC 21/200 with three members at $\sim 160\ h^{-1}$ Mpc, and SC 8/40 with eight members at $\sim 140\ h^{-1}$ Mpc. At low density contrast ($f \geq 2$) these three cores connect to each other through a large cloud of clusters, reaching a total number of 25 members. The Shapley Concentration will be discussed elsewhere (Bardelli et al. 1993, in preparation) with many new redshift data in the region.

SC 29/2 is the Corona-Borealis Supercluster, whose central region has been studied in detail by Postman, Geller, & Huchra (1988).

SC 31/2 is the well-known Hercules supercluster consisting of two cores, identified at high density contrast ($f \geq 200$), which merge into a single unit at low contrast ($f \geq 2$). The reality of this complex, not only in terms of cluster association but also as enhancement and segregation of intracluster galaxies in redshift space has been amply demonstrated (see Freudling, Haynes, & Giovanelli 1988, 1992).

SC 41/2 and SC 43/2, at $\sim 120\ h^{-1}$ Mpc and $170\ h^{-1}$ Mpc, respectively, are the central part of the large filament in Perseus-Pegasus studied by Batuski & Burns (1985a, b). It is worth noting that the extension of this filament toward smaller distances is essentially due to the redshift of A71 adopted by Batuski & Burns ($z = 0.0219$): in fact, if one assumes, as we do, that the redshift of A71 is 0.0717 (Klypin & Kopylov 1983) the Perseus-Pegasus filament splits into two different superclusters. Clearly, measurements of a large number of galaxies in this cluster as well as in the intracluster field are needed to assess the reality of the Perseus-Pegasus complex.

SC 48/2 is the Horologium-Reticulum Supercluster first pointed out by Lucey et al. (1983) and Chincarini et al. (1984), who studied the density excess of galaxies noticed by Shapley (1935) in this region. This supercluster extends roughly in north-south and represents the largest cluster complex in the southern Galactic hemisphere.

4. SUPERCLUSTER ANALYSIS

4.1. *General Properties*

Before applying statistical tests to these superclusters, we have to check their completeness, reliability, and stability. In order to check the completeness of our catalogs, we have analyzed the density of superclusters in 10 shells of constant volume, which we report in Figure 5*a* for $f \geq 2$. From this figure it is clear that the density of superclusters in our catalog decreases significantly for distances larger than $\sim 240\ h^{-1}$ Mpc; a similar trend is visible also for the other catalogs with different f thresholds. The most likely explanation for this trend is the decreasing percentage of measured redshifts at large distances (Fig. 5*b*). The typical 20% uncertainty in the estimated redshifts introduces a spread in the radial distribution of clusters, thus leading to a loss of recognized superclusters at large distances.

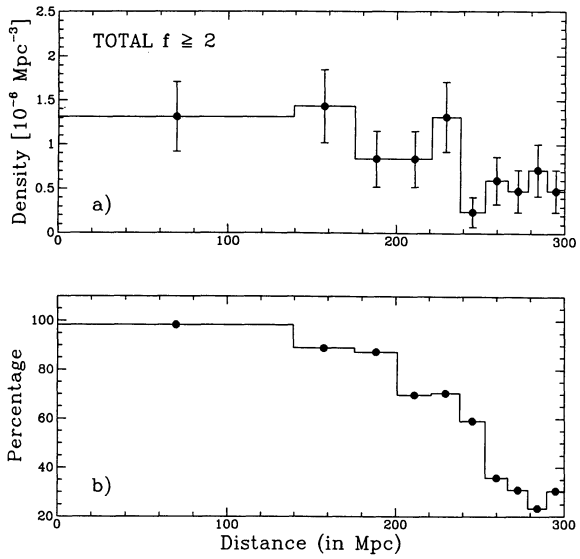

FIG. 5.—(*a*) Density of superclusters (at $f \geq 2$) in 10 shells of constant volume. The 1 σ error bars represent standard Poissonian errors. (*b*) Percentage of clusters with measured redshift as a function of the distance in the Abell-ACO catalog.

The reliability of our superclusters has been checked by constructing random catalogs of clusters with a uniform volume density and the same selection functions as the Abell and ACO catalogs; these catalogs have then been searched for superclusters in exactly the same way as the real data. A comparison between the supercluster lists obtained from the real data and from the average of 100 quasi-random catalogs, with the appropriate selection function, is shown in Figure 6. The four panels of this figure show the supercluster multiplicity function, i.e., the distribution of the number of superclusters with a given number of members, for different values of overdensity ($f \geq 200, 20, 10, 2$). For all the values of f, the real catalog yields a larger number of superclusters with high richness than do the random catalogs. In particular, at high density excesses ($f > 100$) only few binary superclusters are found in the random catalogs, while the real data show not only a large number of binary systems, but also triplets. The difference between real and random data becomes even more evident at intermediate density enhancements ($5 \leq f \leq 100$), where the richness range of the real superclusters increases, while the random systems are substantially triplets at most. For lower density excesses ($f \leq 2$) the number of random triplets becomes comparable with that found in the real data, thus suggesting that there is a high probability that, at these density excesses, a triple system is a random association. In fact, almost all triple systems in the catalog at $f \geq 2$ do not have any correspondence at higher density enhancements (see Table 1). On the contrary,

[1] Actually Shapley (1930) did not realize that the whole region is an exceptionally high cluster density region, but pointed out the exceptionality of one of the cores (SC 21/200) in terms of galaxy density contrast.

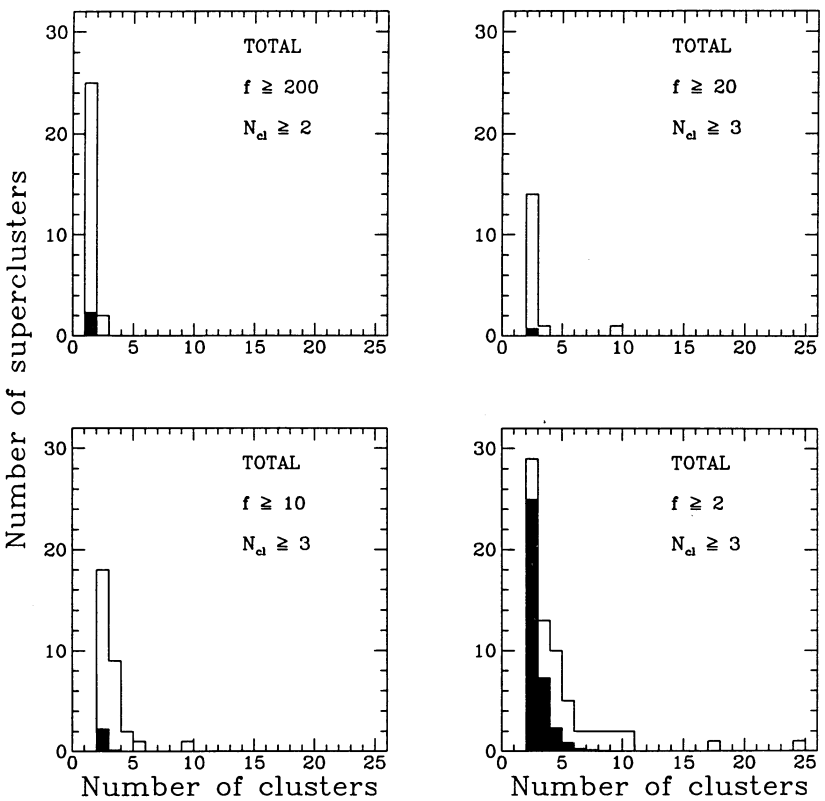

FIG. 6.—Multiplicity function (i.e., number of superclusters with a given number of members) for superclusters at $f \geq 200, 20, 10, 2$. Black histograms represent the results for the average of 100 random catalogs.

almost all triple superclusters found at high density excesses, at $f \geq 2$ are evolved into richer systems. From this comparison, it is clear that a triplet found only at $f \geq 2$ has a high probability of not being physically bound, but a triple system which is already present at high density excesses is likely to be the physical core of a richer supercluster.

Finally, we note two superclusters (the Shapley Concentration and the Horologium-Reticulum complex) which stand out as exceptionally rich concentrations at $f \geq 2$. The Shapley Concentration is already evident at the highest density excesses: the only two superclusters with three members at $f \geq 200$ are in the core of this system, which rapidly grows as f decreases, until it reaches the number of 25 members for $f \geq 2$. At this density excess also the Horologium-Reticulum complex is very prominent: it has only four members at $f \geq 10$ but rapidly grows to 18 members at $f \geq 2$. These two systems are the richest superclusters of our sample and both lie in the southern hemisphere: for this reason in the following we will analyze not only the total sample, but also the Abell and ACO samples separately, in order to better individuate possible differences between the two catalogs.

The third "global" property of our superclusters we checked is their stability or robustness. Because of the way the percolation algorithm works, it is possible that two physically unrelated superclusters are merged together in a single structure in virtue of the presence of a single cluster in-between the two concentrations. To check for this possibility, for each supercluster with $N_{cl} \geq 4$ members we have run N_{cl} times the percolation algorithm by excluding each time one of the members. In the ideal case in which a supercluster would be completely insensitive to the exclusion of any one of its members, a supercluster with N_{cl} members would appear at the end of this procedure N_{cl} times, each time with $N_{cl} - 1$ members. Figure 7 shows the resulting histogram of ΔN for the catalog at $f \geq 2$, where ΔN is the difference between the number of clusters in the original supercluster and the number of clusters still found to be members of the supercluster after eliminating one of the members. If a supercluster breaks into two or more pieces, we

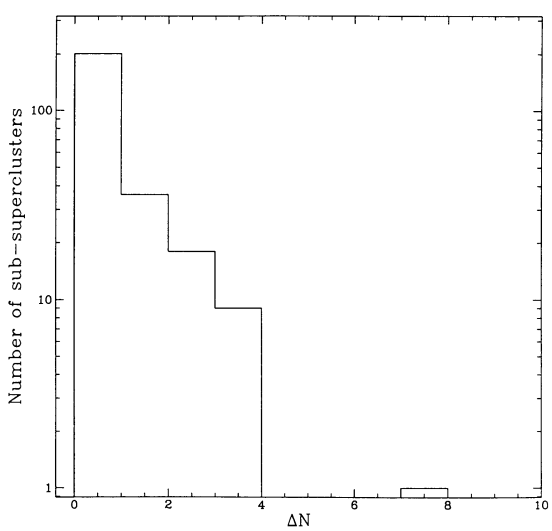

FIG. 7.—Check for the stability of superclusters: ΔN is the difference between the number of members in a given supercluster and the number of members in the greatest sub-supercluster obtained after having eliminated one of the members (see text for details).

have considered ΔN as the difference between N_{cl} and the number of members of the richest resulting group. From the large peak at $\Delta N = 1$ we conclude that most of the systems are largely insensitive to the exclusion of any one of their members. The only interesting exception is the Shapley Concentration, which is totally insensitive to whatever exclusion except for that of A3577, which causes a separation of the supercluster into two substructures of 17 and seven members, respectively.

The fraction of clusters belonging to superclusters as a function of f is shown in Figure 8 for Abell and ACO samples separately: this fraction steadily increases as f decreases and for $f \geq 1.5$ about half of the clusters lie in superclusters. Notice that this fraction for the ACO sample is always higher than that of the Abell one, in particular for high density excesses (larger than 10). This behavior is mostly due to the presence of the Shapley Concentration in the ACO sample. In the same figure we also show the average percentage of clusters in superclusters resulting from 100 random catalogs: this fraction F_{cl}^{R}(SC) not only is always lower than that of the real data, but also decreases more rapidly as f increases and can be very well approximated by $F_{cl}^{R}(SC) \sim 0.59 f^{-1.85}$ for $5 \leq f \leq 40$. Note that the different slope with respect to that given for the same function by Bahcall and Soneira [$F_{cl}^{R}(SC) \sim 6.8 f^{-1}$] is due to the fact that the superclusters in our catalog have $N_{cl} \geq 3$, while theirs have $N_{cl} \geq 2$; moreover their density excesses must be scaled down by a factor ~ 8 in order to be comparable to ours (see § 3.3). If we include in our catalog also superclusters with two members, the above relation becomes $F_{cl}^{R}(SC) \sim 0.77 f^{0.96}$, in good agreement with that of Bahcall and Soneira ($F_{cl}^{R}(SC) \sim 0.85 f^{-1}$), obtained after having scaled down their f.

By subtracting the percentage of clusters in superclusters in the random data from the average (observed) values in the Abell and ACO catalogs, we obtain $24 \pm 3\%$, $24 \pm 2\%$, and $20 \pm 2\%$ for $f \geq 1.5$, 2, and 5. Taken at their face value, these numbers suggest that for $f \leq 5$ the percentage of clusters in superclusters, depurated by the random contamination, is consistent with being constant.

Finally we notice that, although the fraction of clusters in superclusters is quite high at small values of f, the fraction of the total volume occupied by these systems is still very small (Bahcall & Soneira 1984; Tully 1987), reaching about the 2% value at $f \geq 1.5$.

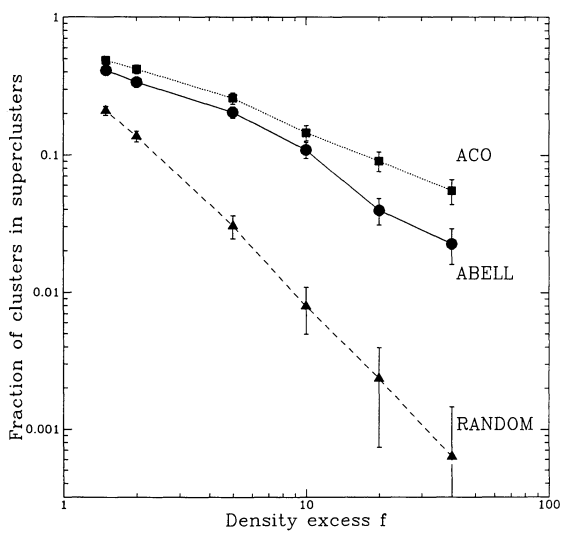

FIG. 8.—Fraction of clusters belonging to superclusters as a function of f: (*circles*) Abell superclusters; (*squares*) ACO superclusters; (*triangles*) average of 100 random catalogs. The 1 σ error bars represent standard Poissonian errors.

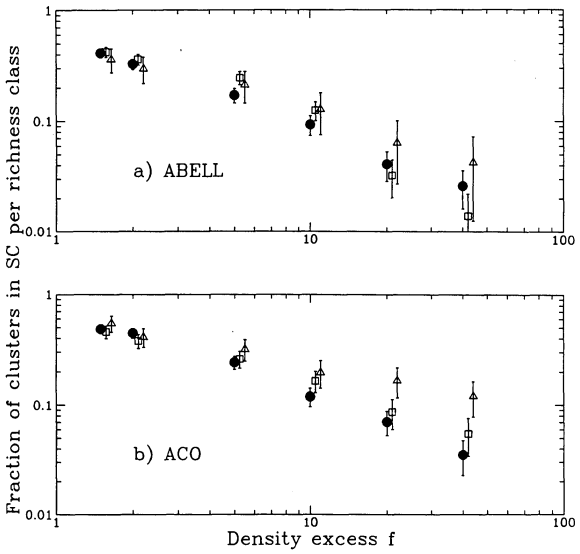

FIG. 9.—Fraction of clusters belonging to superclusters as a function of f, divided into three richness classes; (*circles*) $R = 0$, (*squares*) $R = 1$, (*triangles*) $R \geq 2$. The 1 σ error bars represent standard Poissonian errors. For clarity of representation squares and triangles have been slightly shifted with respect to the abscissa. (*a*) Abell catalog; (*b*) ACO catalog.

It is also interesting to study the percentage of clusters in superclusters as a function of richness. Figure 9 is the same as Figure 8, but with clusters divided into three richness classes (*circles*: $R = 0$; *squares*: $R = 1$; *triangles*: $R \geq 2$). From this figure there is a suggestion that, on average, the richer the clusters are, the higher is their probability of being members of superclusters (for $f \geq 5$). The only exception (even if within the 1 σ error bar) is the $R = 0$ class for the Abell sample, whose probability of being members of superclusters appears to be higher than the $R = 1$ class at high density excesses ($f \geq 20$).

4.2. *Velocity Dispersion in Superclusters*

The possible existence of peculiar motions in superclusters is of great interest for galaxy formation theories and for the determination of the amount of dark matter in these systems. In 1986 Bahcall, Soneira, and Burgett, examining the distribution of cluster pairs in the angular and radial direction, claimed the existence of a strong elongation along the line-of-sight direction, corresponding to a velocity broadening of ~ 2000 km s^{-1} among cluster pairs. But in 1988 Soltan has demonstrated that the Bahcall and Soneira sample is dominated by the Corona-Borealis supercluster, which is elongated along the line-of-sight direction and substantially enhances the mean amplitude of cluster pair elongations in the radial direction. The latter result has been confirmed also by Huchra et al. (1990) and by Postman et al. (1992).

In order to reveal the possible existence of anisotropies in the orientation of the superclusters we have analyzed the distribution of the separations between pairs of clusters belonging to superclusters. We have divided these separations into three components, along the right ascension ($\Delta\alpha$), declination ($\Delta\delta$), and distance (ΔR) directions, and we have studied the scatter diagrams $\Delta\alpha$–ΔR, $\Delta\delta$–ΔR and $\Delta\alpha$–$\Delta\delta$ for all pairs of clusters which are members of superclusters. If peculiar velocities in superclusters are negligible and if the sample is not dominated

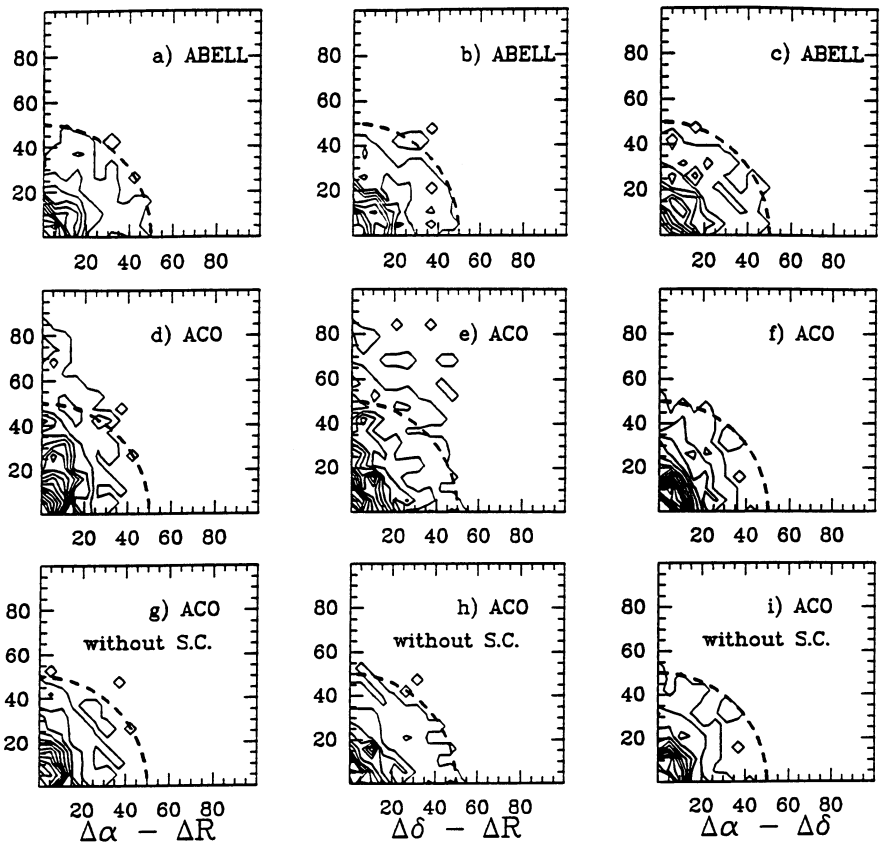

FIG. 10.—Contour diagrams of the separations of pairs of clusters belonging to superclusters: the data are binned in square cells of 5 h^{-1} Mpc and slightly smoothed. In first column $\Delta\alpha$ (x-axis) vs. ΔR (y-axis), in second column $\Delta\delta$ (x-axis) vs. ΔR (y-axis), and in third column $\Delta\alpha$ (x-axis) vs. $\Delta\delta$ (y-axis) for the Abell (*a–c*) and ACO (*d–f*) catalogs and for the ACO catalog without the Shapley Concentration (*g–i*). The dashed curve, which represents an arc of a circle with radius of 50 h^{-1} Mpc, has been plotted to help recognizing the deviations of the data from a circular symmetric distribution.

by structures elongated in a given direction, these scatter diagrams should be symmetric.

In Figure 10 we show, through a contour level representation, the distribution of the pair separations for the Abell (Figs. 10*a*–10*c*) and ACO (Figs. 10*d*–10*f*) samples at $f \geq 2$. For the Abell superclusters there is no evidence of a preferred orientation; on the contrary, the ACO diagrams show a strong elongation in the line-of-sight direction. This effect could in principle be interpreted as a consequence of high peculiar motions of the clusters. However, the ACO sample is dominated by the Shapley Concentration, which is strongly elongated in the radial direction and very rich: ~38% of the total number of pairs of clusters in superclusters of the ACO sample derive from clusters in this concentration. Therefore, we have repeated the diagrams for the ACO sample without the Shapley Concentration (Figs. 10*g*–10*i*): in these figures the elongation has almost completely disappeared, thus confirming that the strong effect seen in Figures 10*d*–10*f* was a consequence of the presence of a very rich system elongated in the radial direction rather than a proof of high peculiar motions in each supercluster.

However, velocity dispersion of clusters in superclusters may exist, and therefore we have tried to quantify it through the histograms of the pair separations $N(\Delta\alpha)$, $N(\Delta\delta)$, and $N(\Delta R)$ that we show in Figure 11 for the Abell (Figs. 11*a*, 11*b*) and ACO (Figs. 11*c*, 11*d*) samples. Once again, there is a clear excess of large ΔR and small $\Delta\alpha$ and $\Delta\delta$ for the ACO pairs: excluding the Shapley Concentration (Figs. 11*e*, 11*f*) this effect is strongly reduced. Notice also that the $\Delta\alpha$ and $\Delta\delta$ distributions are consistent with each other in the Abell sample (a K-S test gives a probability of 49% that they are extracted from the same distribution), but this is not the case for the ACO superclusters, neither from the complete sample ($P = 4 \times 10^{-5}$) nor without the Shapley Concentration ($P = 5 \times 10^{-4}$). This effect is mainly related to the Horologium-Reticulum complex, whose extension in the δ direction is about twice of that in the α direction. Again, being this supercluster very rich, it strongly contributes to the total number of pairs. Excluding also this system from the ACO sample (Figs. 11*g*, 11*h*), the $\Delta\alpha$ and $\Delta\delta$ distributions become consistent with each other ($P = 64\%$). However a lack of small ΔR is still evident in these distributions. This lack can be a consequence of the fact that a non-negligible number of clusters in superclusters, especially for the ACO catalog, do not have measured redshift; the increased uncertainty in the estimated redshifts may well increase the intrinsic ΔR distribution. Indeed, eliminating from the analysis all the superclusters with less than 70% of members with measured redshifts, the difference between the ΔR and the angular ($\Delta\alpha$ and $\Delta\delta$) distributions almost disappears. The final results for the total catalog of superclusters with at least 70% of members with measured redshift, excluding the Shapley Concentration and the Horologium-Reticulum complex, are shown in Figures 11*i* and 11*j*.

In order to quantify and/or set limits on the velocity dispersion within superclusters, we have convolved the observed distributions of $\Delta\alpha$ and $\Delta\delta$, which are unperturbed by peculiar

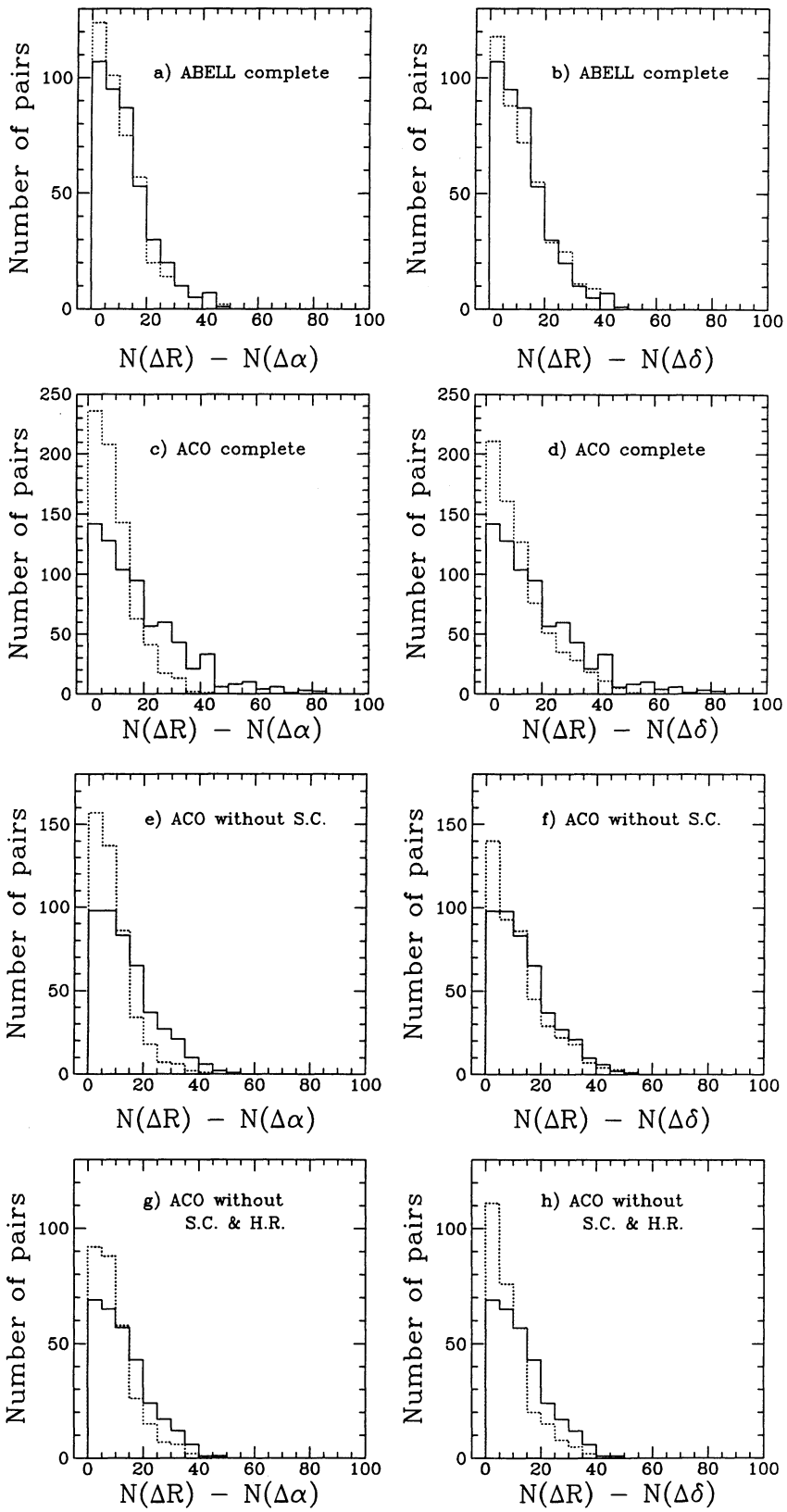

FIG. 11.—Histograms of the pair separations: (*solid line*) $N(\Delta R)$; (*dotted line*) $N(\Delta\alpha)$ or $N(\Delta\delta)$. Comparisons between $N(\Delta R)$ and $N(\Delta\alpha)$ (*first column*) and $N(\Delta R)$ and $N(\Delta\delta)$ (*second column*) for various samples. (*a*, *b*) Abell complete; (*c*, *d*) ACO complete; (*e*, *f*) ACO without the Shapley Concentration; (*g*, *h*) ACO without the Shapley Concentration and the Horologium-Reticulum supercluster; (*i*, *j*) superclusters from the total sample with more than 70% of members with measured redshift and without the Shapley Concentration and the Horologium-Reticulum complex.

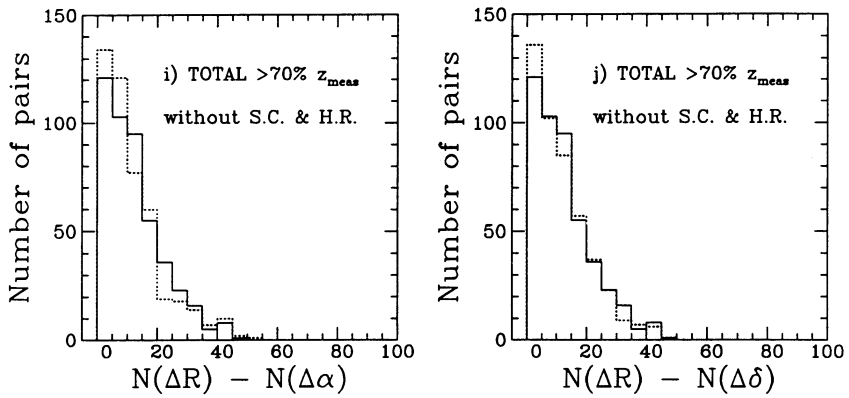

FIG. 11—*Continued*

motions, with a Gaussian velocity distribution. We have then varied the width Δv of the Gaussian velocity distribution and determined the range of Δv for which these convolved distributions are consistent with the distribution observed in the radial direction. Table 3 lists, for each sample, the range of velocity dispersions which are acceptable (at 5% level) according to a K-S test. This table summarizes and quantifies the results seen in Figure 11 and qualitatively discussed above. For the Abell sample the distributions of radial and angular separations are consistent with each other even without any velocity broadening; on the contrary, the ACO sample seems to require a high velocity dispersion to match the two distributions. However, as discussed above, this difference appears to be induced by the orientation of two particularly rich superclusters and disappears after having eliminated them. The final result for the total catalog (Abell + ACO), and using only superclusters with at least 70% of members with measured redshifts, is that the best estimate for the velocity dispersion is ~ 500 km s^{-1} and no velocity dispersion is still consistent with the data; the 2 σ upper limit for the velocity dispersion is of the order of 1000 km s^{-1} (as found by Huchra et al. 1990; Postman, Huchra, & Geller 1992; Nichol et al. 1992). Moreover, if part of the elongation of superclusters is due to a geometrical effect (i.e., to their intrinsic shape), this upper limit should be lowered further on.

From these considerations it is clear that the previous analysis suffers an intrinsic bias: the richer a supercluster is, the higher is its weight. Therefore a single, rich supercluster oriented along the line of sight might lead to the erroneous conclusion that all superclusters are elongated in the radial direction. An alternative method to study the possible elongation along the radial direction is that of analyzing the global shape and orientation of all the superclusters, independently of their richness. This can be done, following West (1989), by studying the inertia tensor of each supercluster, under the hypothesis that these systems are ellipsoids. In order to make this assumption more realistic, the following analysis was restricted to only those superclusters with five or more members. Because of the small number of clusters per supercluster, the derived shapes are especially sensitive to contributions from "peripherical" clusters. In order to reduce this bias, the components of the inertia tensor were computed (following West 1989) as

$$I_{ij} = \sum_{1}^{N_{cl}} \frac{x_i x_j}{r^2}, \qquad (19)$$

where x_i and x_j are the spatial coordinates of a given cluster in a supercluster (with N_{cl} members) and r is its distance from the supercluster centre. Diagonalization of the above matrix yields the three eigenvectors which correspond to the principal axes and give information on their directionality. Then we have computed the angles ϕ_1, ϕ_2, and ϕ_3, defined as the angles between the vector which connects the Earth to the centre of a supercluster and its major, intermediate, and minor axis, respectively. If superclusters are randomly oriented in space, then the values of cos ϕ_1 (and cos ϕ_2 and cos ϕ_3) should be uniformly distributed between 0 and 1, with a mean of 0.5. Therefore an excess of values near cos $\phi_1 \simeq 1$ could suggest that there is a tendency for superclusters to be oriented preferentially along the line of sight. Correspondingly, there should be an excess of values near cos $\phi_2 \simeq 0$ and cos $\phi_3 \simeq 0$, always under the assumption that superclusters are ellipsoids.

In Figures 12*a*–12*c* we report the distributions of cos ϕ_1, cos ϕ_2, and cos ϕ_3 for the total sample of superclusters at $f \geq 2$. Although there seems to be a suggestion of an excess towards cos $\phi_1 \simeq 1$, it is not statistically significant. According to a K-S test there is a probability of $\sim 16\%$ that the observed distribution of cos ϕ_1 is obtained from a uniform distribution ($P \sim 3\%$ for cos ϕ_2 and $P \sim 31\%$ for cos ϕ_3). These probabilities increase to $\sim 20\%$, $\sim 15\%$, and $\sim 47\%$ for cos ϕ_1, cos ϕ_2, and cos ϕ_3, respectively, if we consider only superclusters with more than 70% of members with measured redshift (Figs. 12*d*, 12*e*). Therefore, also from this test we conclude that there is no evidence that superclusters are preferentially elongated along the radial direction.

TABLE 3

RANGES OF VELOCITY DISPERSIONS FOR CLUSTERS IN SUPERCLUSTERS (K-S PROBABILITY $\geq 5\%$)

SAMPLE	RANGE OF VELOCITY DISPERSION (km s^{-1})	
	$N(\Delta\alpha)$–$N(\Delta R)$	$N(\Delta\delta)$–$N(\Delta R)$
Abell complete	0–1100	0–800
ACO complete	1600–2100	1200–1900
ACO without S.C.	1000–1700	200–1300
ACO without S.C. & H.R.	600–1600	700–1600
ACO (>70% z_{meas}) without S.C. & H.R.	0–1300	0–1300
Total (>70% z_{meas}) without S.C. & H.R.	0–1000	0–1000

NOTES.—S.C. = Shapley Concentration; H.R. = Horologium-Reticulum complex.

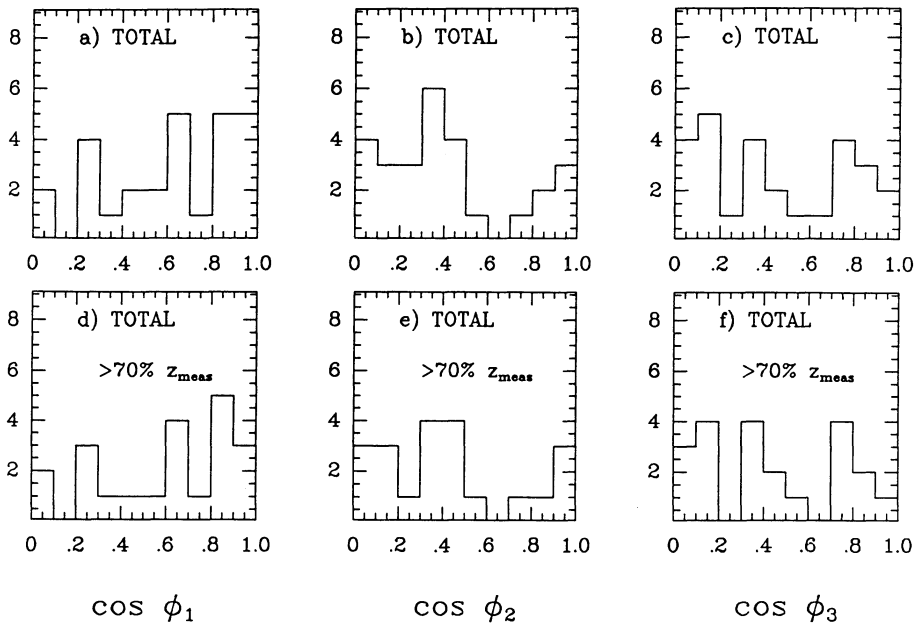

FIG. 12.—Histograms of cos ϕ_1, cos ϕ_2, and cos ϕ_3 for superclusters with five or more members at $f \geq 2$; (*a–c*) total sample; (*d–f*) only superclusters with more than the 70% of members with measured redshift. ϕ_1, ϕ_2, and ϕ_3 are the angles between the line of sight and, respectively, the major, intermediate, and minor axis of a supercluster.

Finally, we note that the use of a variable percolation radius does not influence our results: we have repeated the percolation procedure with constant radii and the resulting superclusters exhibit the same properties we have derived above.

5. SUMMARY

The principal aim of this work has been the construction of an all-sky catalog of superclusters of Abell-ACO clusters at consistent overdensity thresholds, and the study of their properties. The main results can be summarized as follows:

1. We have calibrated a magnitude-redshift relation to assign distance estimates to clusters without measured radial velocity. In particular, we have studied the influence of errors in the original magnitudes and we have taken them into account in our relations, which are reported in equations (6) and (7) for the Abell and ACO catalogs, respectively.

2. We have generated supercluster catalogs at various density excesses f through a percolation algorithm, taking into account also the selection function of the Abell and ACO catalogs.

3. Ranging from high to low f, superclusters steadily evolve from dense cores of few members to richer structures. In particular, two superclusters (the Shapley Concentration and the Horologium-Reticulum complex) stand out as exceptionally rich concentrations. Comparisons with random catalogs establish the physical reality of both the binary (and triple) systems found at high f and the richer structures which appear at lower density excesses.

4. We have studied the distributions of the separations of pair of clusters belonging to superclusters. If there are peculiar motions of clusters in superclusters the distribution of radial separations should be broadened with respect to that of the projected separations. In the ACO sample there seems to exist such an evidence, but this effect is strongly reduced after having excluded from the sample the Shapley Concentration, which is very rich and elongated in the radial direction. After having eliminated "peculiar" superclusters from our sample, we derived an upper limit of ~ 1000 km s^{-1} for velocity dispersion in superclusters.

5. We have studied the inertia tensor of each supercluster and from its eigenvectors we have derived the orientation of its principal axes. Also from this analysis there is no strong evidence for superclusters to be elongated preferentially along the line of sight.

REFERENCES

Abell, G. O. 1958, ApJS, 3, 211 (Abell catalog)
Abell, G. O., Corwin, H. G., Jr., & Olowin, R. P. 1989, ApJS, 70, 1 (ACO catalog)
Bahcall, N. A. 1988, ARA&A, 26, 631
Bahcall, N. A., & Soneira, R. M. 1984, ApJ, 277, 27
Bahcall, N. A., Soneira, R. M., & Burgett, W. S. 1986, ApJ, 311, 15
Batuski, D. J., & Burns, J. O. 1985a, AJ, 90, 1413
———. 1985b, ApJ, 299, 5
———. 1988, ApJ, 335, 542
Cappi, A., & Maurogordato, S. 1992, A&A, 259, 423 (CM)
Chincarini, G., Tarenghi, M., Sol, H., Crane, P., Manousoyannaki, I., & Materne, J. 1984, A&AS, 57, 1
Corwin, H. G., Jr. 1974, AJ, 79, 1356
Ellis, R. S. 1983, in The Origin and the Evolution of Galaxies, ed. B. T. J. Jones & E. J. Jones (Dordrecht: Reidel), 255
Fisher, J. R., & Tully, R. B. 1981, ApJS, 47, 139
Freudling, W., Haynes, M. P., & Giovanelli, R. 1988, AJ, 96, 1791
———. 1992, ApJS, 85, 157
Huchra, J. P., Henry, J. P., Postman, M., & Geller, M. J. 1990, ApJ, 365, 66
Isobe, T., Feigelson, E. D., Akritas, M. G., & Babu, G. J. 1990, ApJ, 364, 104
Klypin, A., & Kopylov, A. 1983, Sov. Astron. Lett., 9, L41
Lucey, J. R., Dickens, R. J., Mitchell, R. J., & Dawe, J. A. 1983, MNRAS, 203, 545
Mattig, W. 1958, Astron. Nach., 284, 109
Nichol, R. C., Collins, C. A., Guzzo, L., & Lumsden, S. L. 1992, MNRAS, 255, 21P
Postman, M., Geller, M. J., & Huchra, J. P. 1988, AJ, 95, 267
Postman, M., Huchra, J. P., & Geller, M. J. 1992, ApJ, 384, 404 (PHG)
Postman, M., Huchra, J. P., Geller, M. J., & Henry, P. 1985, AJ, 90, 1400
Osmer, P. S. 1981, ApJ, 247, 762

Raychaudhury, S. 1989, Nature, 342, 251
Rood, H. J. 1992, MNRAS, 254, 67
Scaramella, R., Baiesi-Pillastrini, G., Chincarini, G., Vettolani, G., & Zamorani, G. 1989, Nature, 338, 562
Scaramella, R., Zamorani, G., Vettolani, G., & Chincarini, G. 1991, AJ, 101, 342 (SZVC)
Shanks, T., Stevenson, P. R. F., Fong, R., & Mac Gillivray, H. T. 1984, MNRAS, 206, 767
Shapley, H. 1930, Harvard Obs. Bull., 874, 9
———. 1935, Ann. Harvard Coll. Obs., 88, 107
Soltan, A. 1988, MNRAS, 231, 309
Struble, M. F., & Rood, H. J. 1991, ApJS, 77, 363
Thuan, T. X. 1980, in Physical Cosmology, Les Houces Session XXXII, ed. R. Balian, J. Audouze, & D. Schramm (Amsterdam: North-Holland), 277
Tully, B. R. 1986, ApJ, 303, 25
———. 1987, ApJ, 323, 1
Tully, B. R., Scaramella, R., Vettolani, G., & Zamorani, G. 1992, ApJ, 388, 9
Vettolani, G., Chincarini, G., Scaramella, R., & Zamorani, G. 1990, AJ, 99, 1709
Weinberg, S. 1972, Gravitation and Cosmology (NY: Wiley)
West, M. J. 1989, ApJ, 347, 610